15th IFK
Proc. of the 15th International Fluid Power Conference <Symposium/Conference>
<DOI>

Radial flow force reduction in hydraulic spool valve using balanced through-hole design

Yuhang Zhang, Shipei Zheng, Jiaxi Zhang,
Jianshe Feng, Miao Yang, Guangwei Zhang, Beichen Ding*

School of Advanced Manufacturing & Southern Marine Science and Engineering Guangdong Laboratory (Zhuhai), Sun Yat-sen University, People's Republic of China
**Corresponding author: E-mail address: dingbch@mail.sysu.edu.cn*

Abstract.

Hydraulic spool valve (HSV) is a key regulating component in fluid power systems owing to its capability for precise flow and pressure control. Unbalanced radial flow force (RFF) is a major contributor to spool instability and friction-induced failure, particularly in open-neutral configurations where flow field asymmetry is prominent. Although conventional design assumes that radial forces are self-balanced due to geometric symmetry, practical valve structures constrained by standardized port layouts frequently induce asymmetric pressure and velocity distributions. To address this issue, a novel balanced through-hole design is proposed and integrated into the mid-shoulder region of the spool. Computational fluid dynamics (CFD) simulations are employed to investigate the generation mechanism of RFF and to evaluate the effectiveness of the proposed structure. The Realizable k-ε turbulence model is adopted to capture the dominant turbulent features, and the individual contributions of pressure and viscous forces to the RFF are quantified. A parametric study is conducted to examine the influence of through-hole inclination angle on force reduction performance. The study results indicate that RFF is predominantly pressure-driven, accounting for more than 85% of the total force, with pronounced asymmetry concentrated in the mid-shoulder region. By introducing a dual through-hole structure inclined at 15°, the RFF acting on the mid-shoulder is reduced by 45.5%, while the total spool RFF is decreased by 29.9%. The proposed design effectively improves flow symmetry and suppresses local pressure gradients, providing a practical solution for RFF mitigation in compact hydraulic spool valves.

Keywords. Hydraulic spool valve, Radial flow force, Through-hole design, CFD simulation, Structural optimization.

1. INTRODUCTION

Hydraulic systems are extensively applied in critical engineering domains such as construction machinery, marine equipment, and aerospace, where they serve as core components in applications, e. g. electric loader bucket and boom drive control [1]. These systems are valued for their rapid response, high power density, and precise controllability [2]. As a core regulating component within a hydraulic system, hydraulic valve plays a pivotal role in determining system responsiveness, stability, and energy efficiency. Among them, the hydraulic spool valve (HSV) employing thin-walled orifice structures exhibit reduced sensitivity to oil viscosity and temperature variations, making them widely used in advanced components such as proportional and servo valves [3].

The spool-to-sleeve clearance of HSVs typically ranges between 5 to 20μm, serving functions such as clearance sealing and motion guidance [4]. Ideally, axial movement of the spool should only induce minimal and stable friction. However, in practical applications, hydraulic forces, thermal deformation, and particulate contamination alter the lubrication state [5], leading to spool hysteresis, jamming, or stiction. Such phenomena can significantly deteriorate control performance and, in severe cases, induce valve failure or safety incidents [6]. Consequently, understanding and mitigating spool stagnation has become a critical issue in hydraulic valve research, traditionally attributed to unbalanced flow forces and lubricant viscosity effects.

Among the influencing factors, flow force is widely recognized as one of the primary contributors to control performance degradation [7]. HSVs regulate flow direction and magnitude through axial displacement of the spool. When the orifice formed between the spool shoulder and sleeve is partially opened, fluid acceleration occurs, which alters the flow momentum and generates force on the spool. Flow force is commonly categorized into steady-state and transient components. The transient component is usually considered negligible compared to the steady-state force. When fluid flows through the throttle port, it experiences changes in velocity and direction, resulting in hydraulic forces on the spool surface, both in axial and radial directions [8].

While research on axial flow force has matured, the radial flow force (RFF) has received relatively limited attention. Many studies have assumed that due to geometric symmetry, RFFs are self-balanced and can be neglected [9]. However, in actual engineering designs, the flow chamber geometry is often asymmetric. This asymmetry results from practical constraints related to valve block layout and standardized port configurations, especially for base-mounted HSVs that follow ISO mounting standards. These designs lead to uneven pressure and velocity distributions along the cylindrical surface of the spool and the annular gap between spool and sleeve [10]. The resulting unbalanced RFF may push the spool toward one side, causing increased friction and possible motion failure.

To mitigate RFFs, researchers have developed a variety of structural modifications. One common method involves machining circumferential pressure-equalizing grooves on the spool shoulder to improve pressure distribution. Hong et al. proposed the use of spiral grooves along the spool surface [11]. These grooves enable simultaneous axial and circumferential pressure release, which effectively reduces pressure peaks and lowers total RFF by over 60 percent. Han et al. introduced a guide groove connected to a central pressure-equalizing groove, which distributed pressure more uniformly and enhanced the response frequency of the valve [12]. Additionally, the shape of the spool edge, such as right-angle, conical, or curved forms, influences the throttle jet direction and thereby affects the RFF at the outlet [13]. However, experimental results show that in many cases, the inlet section's RFF remains largely unchanged despite structural modifications.

Most existing studies focus on negative-opening HSVs, whereas open-neutral configurations remain underexplored. Moreover, complex multi-step throttling structures, such as claw-shaped notches [14], limit the applicability of circumferential balancing grooves. Importantly, traditional groove-based methods act as passive compensation mechanisms, redistributing pressure after radial forces have already developed. In contrast, the present study aims to suppress RFF at its point of origin. By introducing pressure-relief through-holes directly within the spool shoulder, where jet impingement and pressure stagnation occur, the proposed design aims to suppress the formation of pressure asymmetry rather than redistributing it downstream.

2. PHYSICAL MODEL DESCRIPTION

The typical multi-way spool valve (MSV) working principle and structure of the loader hydraulic system are shown in Figure 2.1. Positioned within the main hydraulic circuit, the MSV dis-tributes flow from the main pump to the boom/bucket cylinders, enabling efficient operation of the work equipment. The MSV features a series-parallel integrated two-section design, structurally composed of the valve body, bucket spool valve section, boom spool valve section, and check valves, as shown in Figure 2.1(a). The inlet of two sections is arranged in series, granting priority to the bucket section from Figure 2.1(b). When the bucket section active, it prevents simultaneous operation of the boom section. The return oil passages adopt a parallel configuration, allowing both sections to return oil concurrently.

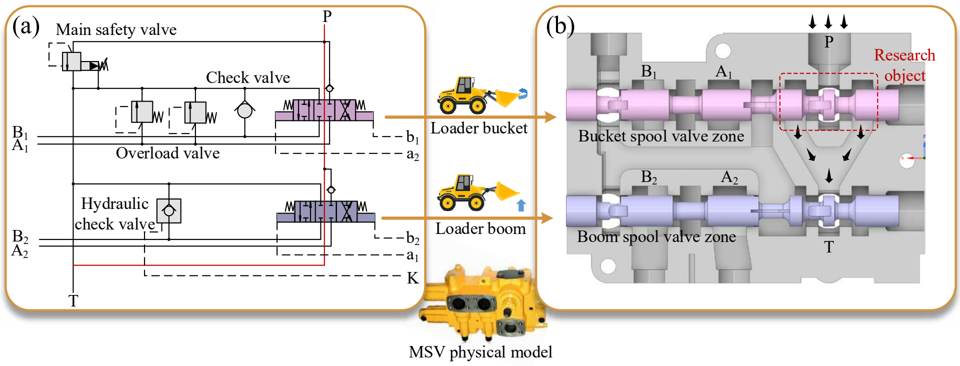

Figure 2.1. MSV working principle and structure of the loader hydraulic system: (a) Working principle; (b) Valve structure.

Due to the asymmetric and discontinuous internal flow passage geometry, the fluid develops an unbalanced turbulent flow. This generates uneven fluid pressure distribution on the spool surface, resulting in unbalanced RFFs. Furthermore, the unbalanced RFF tends to induce spool tilting, leading to asymmetric variation in the clearance between the spool and valve body. In severe cases, this may cause direct contact between the spool and valve body, significantly increasing frictional resistance during spool movement and potentially resulting in sticking or even complete seizure. Specially, when high-pressure fluid enters the valve chamber, it initially impacts the shoulder of the P-T flow path on the spool. Thus, this paper focus on the unbalanced RFF mechanism and reduction approach based on the P-T flow path of the bucket spool valve. The simplified HSV geometry is shown in Figure 2.2.

This study investigates a full circumferential opening spool valve, whose structural characteristics are illustrated in Figure 2.2(a). The HSV is composed of valve body and valve spool. Specially, as shown in Figure 2.2(b), the valve spool mainly consists of five components. Hydraulic fluid enters through the inlet, passes through four throttling orifices, and exits via both left and right outlets (as shown in Figure 2.2c). The valve body and spool exhibit strict bilateral symmetry. When the spool is in its neutral position, x_{01}=x_{04}=0.4 mm and x_{02}=x_{03}=0.35 mm.

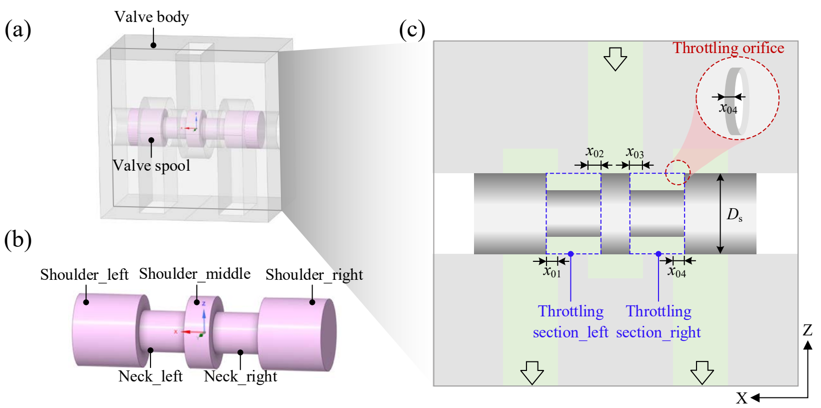

Figure 2.2. Object HSV structure: (a) HSV assembly drawing; (b) Valve spool structure; (c) Central cross-section view. In (c), x_{01} ~ x_{04} represent valve port openings between the valve body and spool shoulders, and D_s is the spool shoulder diameter.

3. NUMERICAL SIMULATION

3.1. Computational fluid domain

The main valve structure is simplified and the extracted fluid domain is shown in Figure 3.1(a). It is a symmetric structure and thus the fluid domain can be simplified as a half to decrease simulation time, shown in Figure 3.1(b). The boundary condition status is shown in Figure 3.1(c) to satisfy the realistic working condition and symmetry flow field.

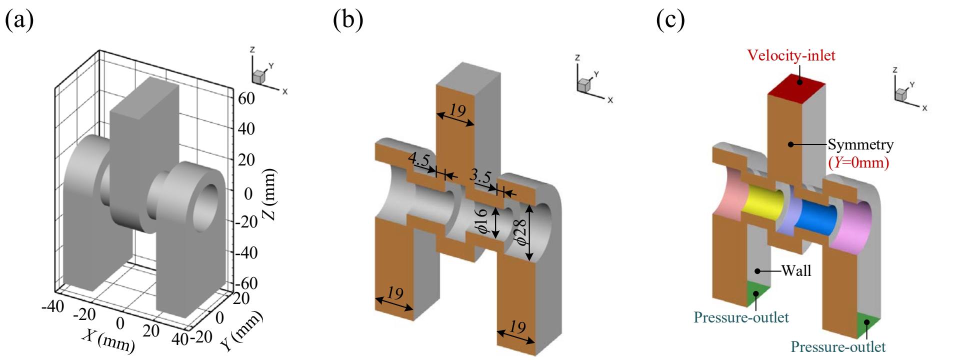

Figure 3.1. Fluid domain model and key structure size: (a) Complete fluid domain; (b) One-half fluid domain from x-axis; (c) Fluid domain boundary condition settings.

3.2. Meshing and independence verification

This investigation employs ANSYS Fluent® software to perform numerical simulations associated with HSVs. Compared to structured grids, unstructured grids are more efficient and easier to control in terms of grid numbers. Given the complex configuration of the HSV's orifice and its compact volume, the entire computational domain is divided into a three-dimensional unstructured mesh using Fluent Meshing® software to ensure grid quality and improve computational efficiency. To capture complex turbulence behaviour such as high-speed jet of valve ports and vortex, five 'Body of Influence' (Boi) regions are developed to refine the mesh, which are shown in Figure 3.2(a). Consequently, at least four mesh models of varying densities are produced in one fluid domain.

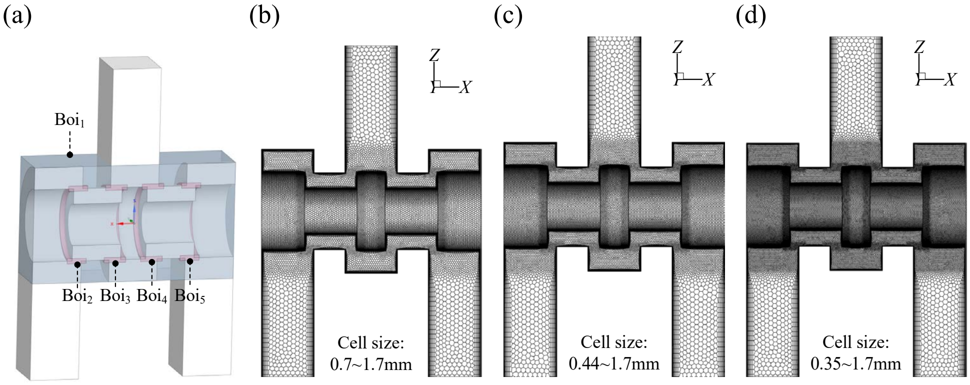

Figure 3.2. Boi regions setting for mesh refinement and mesh quantity comparison: (a) Boi regions setting for mesh refinement; (b) Mesh A with cell size 0.7~1.7mm; (c) Mesh B with cell size 0.44~1.7mm; (d) Mesh C with cell size 0.35~1.7mm.

Table 3.1. Mesh independence verification setting

Region	Mesh A	Mesh B	Mesh C
Overall size (mm)	1.70	1.70	1.70
Boi_1 size (mm)	1.20	0.75	0.60
Boi_2 size (mm)	0.70	0.44	0.35
Boi_3 size (mm)	0.80	0.50	0.40
Boi_4 size (mm)	0.80	0.50	0.40
Boi_5 size (mm)	0.70	0.44	0.35

Mesh division is a pivotal factor in numerical simulations, with the number of meshes directly impacting computational accuracy and determining the convergence and correctness of residual results. Consequently, to guarantee calculation precision and enhance efficiency by reducing computation time, it is imperative to assess the mesh density's relevance prior to the commencement of calculations. The mesh independence test is conducted for a steady simulation. Three mesh models of varying densities are produced, as depicted in Figure 3.2(b)-(d). The detailed mesh setting of different Boi regions is shown in Table 3.1. When the liquid flows at a velocity of 4.8733 m/s, the model with three different mesh numbers is calculated with the outlet pressure set to 0 MPa as the boundary condition. The pressure of inlet (P_{in}) and the radial fluid force (F_r) on the valve core are monitored for the mesh independence. The final results of the mesh independent verification and the error of mesh independence index are presented in Table 3.2. As observed from Table 3.2, an increase in the number of grids leads to a closer alignment between the monitored P_{in} and F_r. When the mesh quantity is increased to 841 908, the error of P_{in} and F_r are at 0.33% and 0.14%, which has been maintained within 0.5%. For a better radial fluid force mechanism revealing and faster computation speed, Mesh C is chosen for the subsequent simulation.

Table 3.2. Mesh independence verification results

Mesh type	Mesh elements	Inlet pressure (Pa)	% Change	Spool RFF (N)	% Change
Mesh A	219 473	61764.3	--	1.436	--
Mesh B	524 611	61006.4	1.20%	1.405	2.20%
Mesh C	841 908	60803.2	0.33%	1.406	0.14%

The selection of the turbulence model and near-wall mesh strategy is guided by the specific flow characteristics of the HSV rather than an assumption of fully developed turbulence. Although hydraulic oil exhibits relatively high viscosity, the flow inside the valve is dominated by strong acceleration through narrow throttling orifices, high velocity gradients, and jet–wall interactions, which promote locally turbulent and separation-dominated flow structures even at moderate Reynolds numbers

In regards to the near-wall approach for Realizable k-ε, the particular complexity of the valve geometry leads to the separation and reattachment of boundary layer easily. For this reason, the ‘enhanced wall treatment’ (EWT) is employed in the present work, which solves viscous substrates directly for the large pressure gradient of the valve port [15]. The number of boundary layers is 10, and the growth ratio is 1.2. The critical value of $y+$ of the fluid domain wall, which signifies the non-dimensional wall distance, is currently maintained below 5. This configuration enables adequate resolution of near-wall pressure gradients and wall shear stresses without excessive mesh refinement. Mesh independence verification further confirms that the selected turbulence model and boundary layer settings yield stable predictions of inlet pressure and radial flow force, with variations below 0.5%, indicating that the numerical results are not unduly sensitive to the chosen near-wall discretization.

3.3. Physical properties and boundary conditions

In this investigation, the calculation is performed under steady-state conditions. The physical properties of liquids used in the simulation are shown in Table 3.3.

Table 3.3. Physical properties and boundary conditions for the CFD simulations

Targets			Values or settings
Physical properties	Hydraulic oil L-HM46	Temperature (°C)	40
		Density (kg/m^3)	870
		Viscosity (Pa·s)	0.04
Boundary conditions	Inlet	Velocity (m/s)	4.8733
	Outlet	Pressure (MPa)	0
	Symmetric face	Symmetry	--
	Valve body Valve spool	Wall	No-slip and adiabatic

Monitoring faces are established at the inlet/outlet positions of the throttle holes to monitor pressure pulsations and flow rate pulsations. These data points are utilized to assess the stability of the calculation results and will be compared and analysed with the experimental findings at a subsequent stage. The boundary condition status is shown in in Figure 3.1(c) to satisfy the realistic working condition and symmetry flow field. Given that the HSV possesses a stable structure and its internal flow dynamics are solely determined by the inlet and outlet boundary conditions, velocity-inlet and pressure-outlet conditions are employed for the calculations while assuming an adiabatic wall surface and no-slip condition.

3.4. Solution strategy

The pressure-based solver is used in the solution. Different discretisation formats are used for the control equation terms to accelerate convergence, 'Least Square Cell Based' discretisation for the gradient term, 'PRESTO!' for the pressure term, 'Second Order Windward' discretisation for the momentum term and each turbulence term. The final discretised control equations are solved by 'Coupled' algorithm. Especially, these parameter settings are verified stable in many HSV simulations. In the simulation process, convergence is deemed to have been achieved when the corresponding parameters within an identical grid cell remain invariant between two successive calculations. Nevertheless, this ideal condition is seldom encountered in practical computations. To affirm the convergence of computational results, the following criteria are typically satisfied: (1) the residual value of the continuous equation should be less than 10^{-5}, with a remaining residual value of less than 10^{-6}; (2) monitor changes such as spool RFF within the fluid domain are less than 0.5%.

4. RESULTS AND DISCUSSION

4.1. Spool radial unbalanced flow force analysis

Before analysing the radial unbalanced force characteristics within the HSV, the flow characteristics of the flow channel should be given. Therefore, the average velocity of the centre cross-section (Y=0 mm) just as Figure 3.1(c) of the valve is first obtained, as shown in Figure 4.1.

Since the hydraulic oil flow inside the valve chamber is restricted by the walls of the spool and the valve body, distinct flow characteristics can be observed. The flow zone division and flow characteristics are shown in Figure 4.1(a) and (b). As the oil enters through the inlet, firstly a part of the oil impinges on the middle shoulder (region A_1), secondly the convergence enters the inlet throttling port (region A_2) and forms a free jet, and then it collides with the wall of the valve neck (region A_3) to form a wall jet region. Next, the wall jet enters the outlet throttling port (region A_4), where the chamber area increases, allowing the jet to fully develop, which is called the outflow jet region. When the outflow jet contacts the wall, another wall jet begins to form, which has a lower velocity magnitude and a wider jet width than the previous wall jet region. At the same time, a portion of the oil is trapped in the narrow region formed by the spool shoulder and the valve body (region A_5), forming a strong vortex.

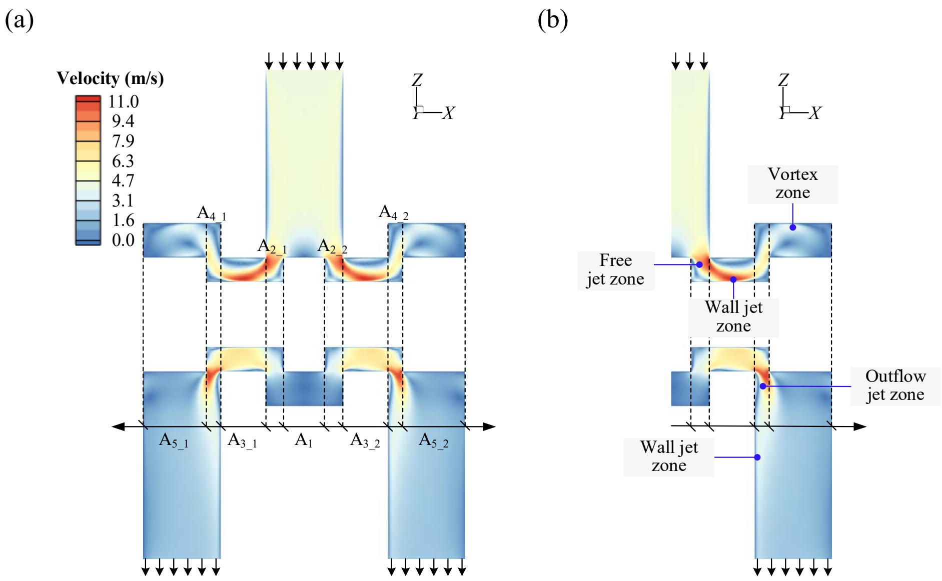

Figure 4.1. Average velocity and flow characteristics of the centre cross-section (Y=0 mm): (a) Flow zone division; (b) Flow characteristics. Especially, due to the symmetrical velocity contour distribution of the left and right parts, figure (b) only shows the right fluid domain.

The RFF is dominated by the pressure component and the viscous component, and Figure 4.2 shows the values and percentages of these two components in the Z-direction for different wall parts (W_1-W_5). Due to the symmetrical contour distribution of the spool wall left and right parts, pressure and WSS-Z contours are placed in a separate contour. From Figure 4.2(a) and (b), the RFF on each spool wall is mainly dominated by the pressure force component, and the viscous force only has a certain contribution (23%) in the middle shoulder (W_1), while the viscous force in the rest walls accounts for less than 10%. Among them, valve neck wall jet zones ($W_{3\text{-}1}$ and $W_{3\text{-}2}$) are the main positive RFF sources, showing significant positive pressure force component (3.34 N), and the viscous force contribution is small but in the same direction (+Z). Conversely, outlet shoulder zones ($W_{5\text{-}1}$ and $W_{5\text{-}2}$) show the most significant negative RFF (-4.28 N). Especially, the middle shoulder (W_1) has a smaller force value but possesses the opposite viscous force direction.

In short, the overall spool wall exhibits positive RFFs, with pressure still dominating (89% of the total). The above analyses indicate that there is a significant pressure asymmetry in these zones, which is the main source of unbalanced RFFs. In addition, since the spool is in the neutral position, the RFF on each region of the spool is symmetrically distributed, further indicating that the simulation is reliable by taking 1/2 flow domain as Figure 3.1.

It should be noted that the pressure values reported in this study are expressed in terms of gauge pressure, with the outlet pressure specified as 0 MPa. Under this formulation, negative pressure values may appear in regions of strong flow acceleration, jet impingement, or local flow separation. These negative values represent pressure levels lower than the outlet reference pressure and do not correspond to negative absolute pressures.

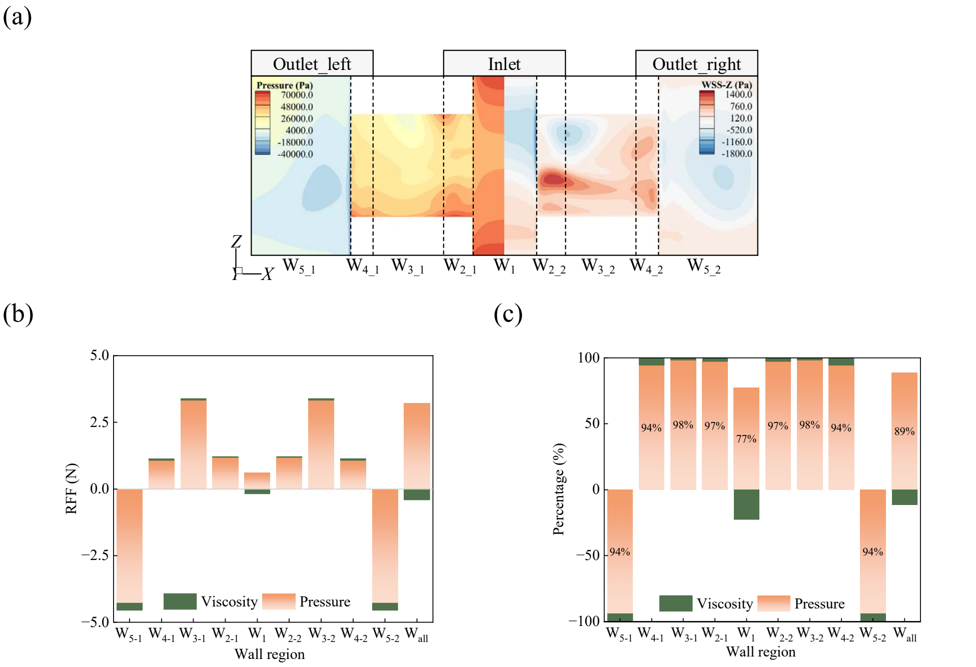

Figure 4.2. Pressure and viscous components of RFF on the spool wall and their proportion: (a) Spool walls division; (b) Pressure and viscous force value; (c) Pressure and viscous force value proportion. Especially, figure (a) exhibits the wall pressure and *Z*-direction wall shear stress (WSS-*Z*) in the *XOZ* view.

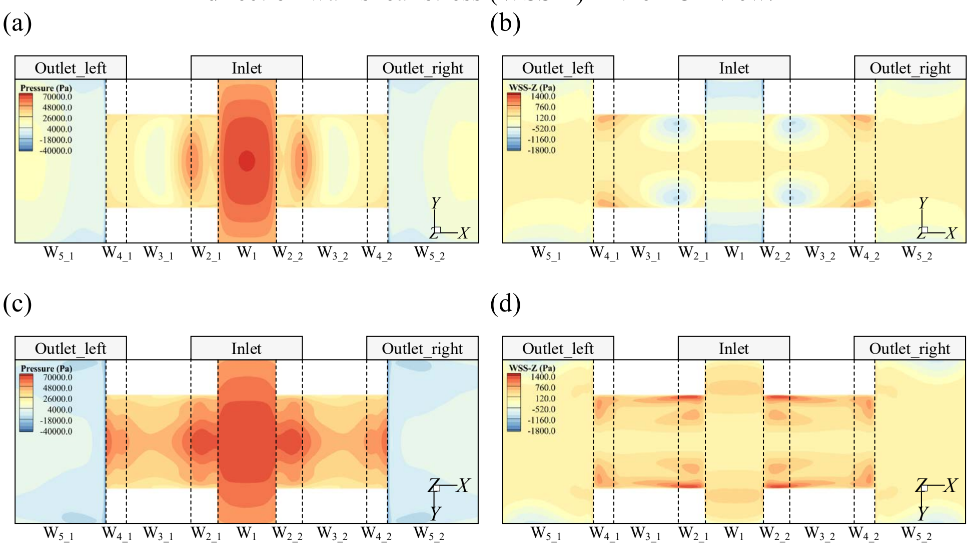

Figure 4.3. Pressure and WSS-*Z* distribution of the upper and lower spool walls: (a) and (b) Pressure and WSS-*Z* distribution of the upper spool wall; (c) and (d) Pressure and WSS-Z distribution of the lower spool wall.

The wall pressure and *Z*-direction wall shear stress (WSS-*Z*) of the upper and lower spool walls in Figure 4.3 further reveal the asymmetry in the spatial distribution of pressure and shear stress. From Figure 4.3 (a) and (c), a more pronounced pressure difference is visible at the upper and lower walls in W_3, corresponding to the larger radial positive force here in Figure 4.2. In W_5, the lower spool wall pressure decreases significantly, creating a significant negative RFF. In contrast, the high WSSs shown in Figure 4.3 (b) and (d) are mainly concentrated in the throttling regions of W_2 and W_4, and despite the large local gradients, their values are much lower than the pressure differences, verifying that the contribution of viscous forces is relatively small.

4.2. Spool radial unbalanced flow force reduction

Above analysis of pressure distribution relative to the middle shoulder clearly reveals that elevated pressure difference predominantly occurs within the central region of the upper and lower walls. To effectively reduce unbalanced RFF, optimization of these specific areas is required. Figure 4.4(a) shows the original valve spool (D_0). Figure 4.4(b) presents an optimized model (D_1) incorporating two perpendicular through-holes (diameter: 2.5 mm) positioned at the mid-section of the shoulder. This design aims to minimize the pressure differential between the upper and lower wall surfaces, thus reducing the unbalance RFF.

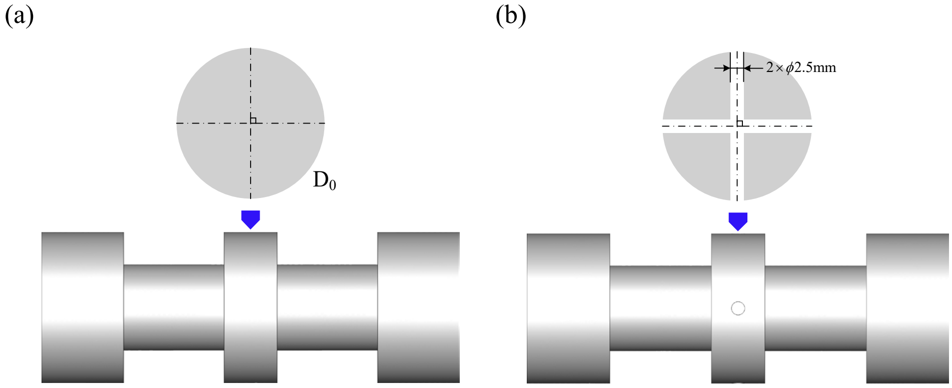

Figure 4.4. Original and optimized valve spool: (a) Original valve spool D_0; (b) Optimized valve spool D_1 with two perpendicular ϕ2.5mm through-holes.

4.2.1. Effect of balanced through-holes structure

Figure 4.5(a) and (b) shows the wall RFF components of two different shoulder structure. The optimized model shows a 20.3% decrease in pressure component, a 15.5% decrease in viscosity component and a 22.8% decrease in net RFF compared to the original model. It is shown that the balanced through-hole structure effectively guides the fluid diversion through the orifice and reduces the pressure gradient and shear effect of the shoulder upper and lower walls, thus weakening the unbalanced RFF. For the entire spool, the pressure component is reduced by 7.3%, the viscous component by 7.0%, and the combined force by 7.3%. Although the overall RFF change is relatively small, the local optimisation effect of the shoulder region is significant. This study is more concerned with an analysis of the effect of pressure on the middle shoulder, given the high pressure-RFF share.

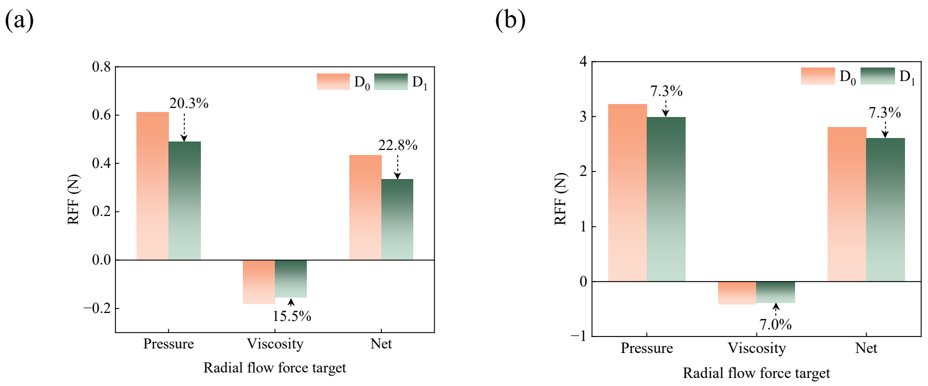

Figure 4.5. RFF on the middle shoulder wall (W_1) and the overall spool (W_{all}) of spools D_0 and D_1: (a) RFF components on the W_1; (b) RFF components on the W_{all}.

Pressure distribution on the upper and lower walls of two shoulder models are shown in Figure 4.6. It can be found that the centre area of the upper and lower walls shows an elliptical high-pressure region, and the boundary pressure decreases abruptly, indicating that the main flow passes around the shoulder resulting in a pressure build-up at the stagnation point. Meanwhile, the area of the high-pressure region on the lower wall is larger than that on the upper, especially at the edge position, resulting in a radial pushover trend (Figure 4.6a and b). With the interference of the through-holes structure, the pressure at the centre is effectively released as the pressure relief channel guides the fluid across the convex shoulder (Figure 4.6c and d). The reduction of the high-pressure areas improves the symmetry and balance of the upper and lower walls, which helps to reduce the RFF difference.

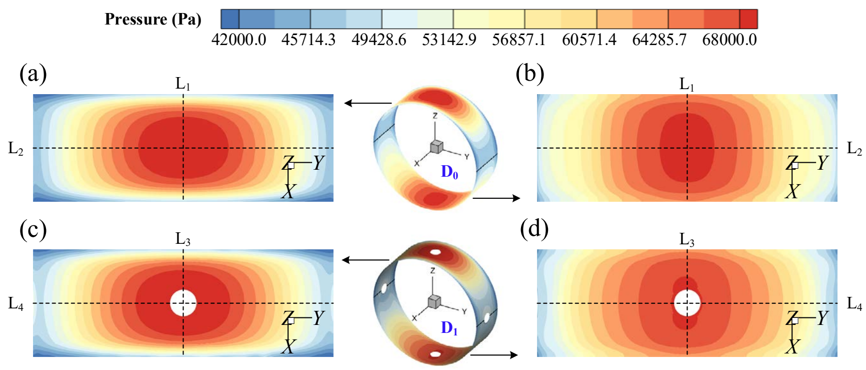

Figure 4.6. Pressure distribution on the upper and lower walls of two shoulder models: (a) and (b) Pressure distribution on the upper and lower walls of D_0; (c) and (d) Pressure distribution on the upper and lower walls of D_1.

The pressure values on the vertical bisectors (L_1~L_4) of the upper and lower walls are further extracted, as shown in Figure 4.7. From Figure 4.7(a), the optimisation resulted in an overall decrease in the lower wall (L_3) pressure and an overall increase (L_1) in the upper wall pressure. Meanwhile, the pressure difference of L_3-L_1 can be found in Figure 4.7(b). It can be found that the positive (+*Z*) pressure difference is reduced as a whole (near $-5<X<-3$mm and 3<X<5mm), and the negative (-*Z*) pressure difference is increased (near -3<X<3 mm), which indicates the positive RFF decrease (+*Z*) as the negative RFF (-*Z*) increase. Then, the overall RFF decrease (+*Z*). The polar plots of L_2 and L_4 are shown in Figure 4.7(c) and (d). The inhomogeneity is defined to measure the pressure difference, which is shown as

$$\sigma_i = \frac{\left| A_{\text{lower}} - A_{\text{upper}} \right|}{A_{\text{lower}}} \times 100\% \tag{4.1}$$

where A_{lower} and A_{upper} are closed curve area enclosed by L_2 and L_4 and the coordinate axes, *i* represents the spool model.

Specially, $\sigma_0 = 1.39\%$ and the $\sigma_1 = 0.67\%$, which indicates that the overlapping cross area of the graph lines increases and the radial symmetry is enhanced after optimisation.

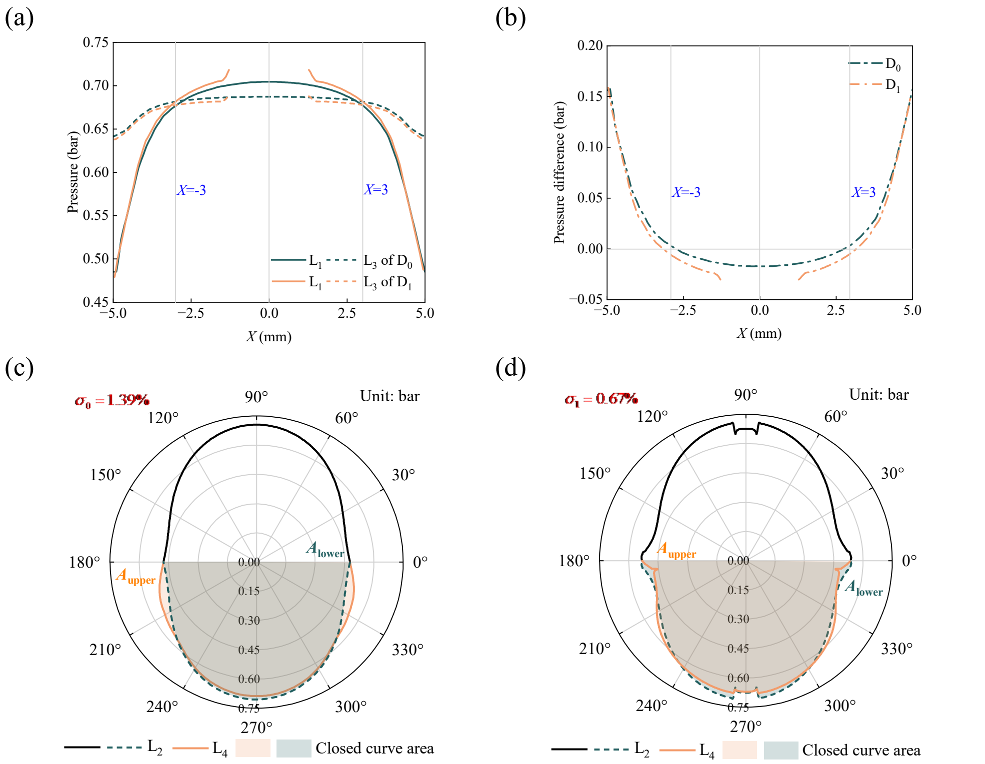

Figure 4.7. Pressure value extracted from L_1~L_4 of the shoulder D_0 and D_1 walls: (a) Pressure value extracted from L_1 and L_3; (b) Pressure difference of L_1 and L_3; (c) Polar plots from L_2 and L_4 on model D_1; (d) Polar plots from L_2 and L_4 on model D_2. Especially, in figure c and d, the cross areas are drawn for identifying the pressure difference between L_2 and L_4.

4.2.2. *Effect of balanced through-hole angle*

In this section, the effect of different through-hole angles on the suppression of radial unbalance force is comparatively analysed. The four through-hole angle models used in this study are shown in Figure 4.8. They are named as model D_0~D_4.

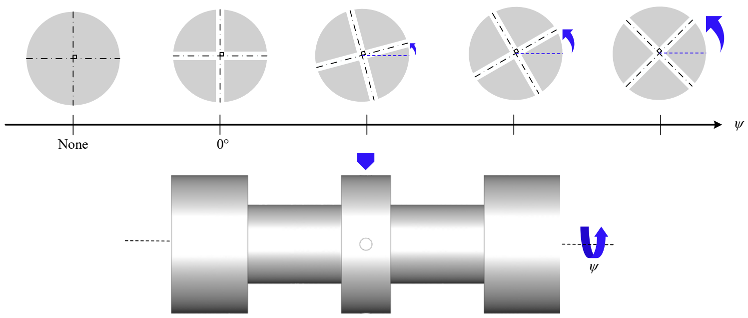

Figure 4.8. Original model and four different balanced through-holes angle (ψ) models.

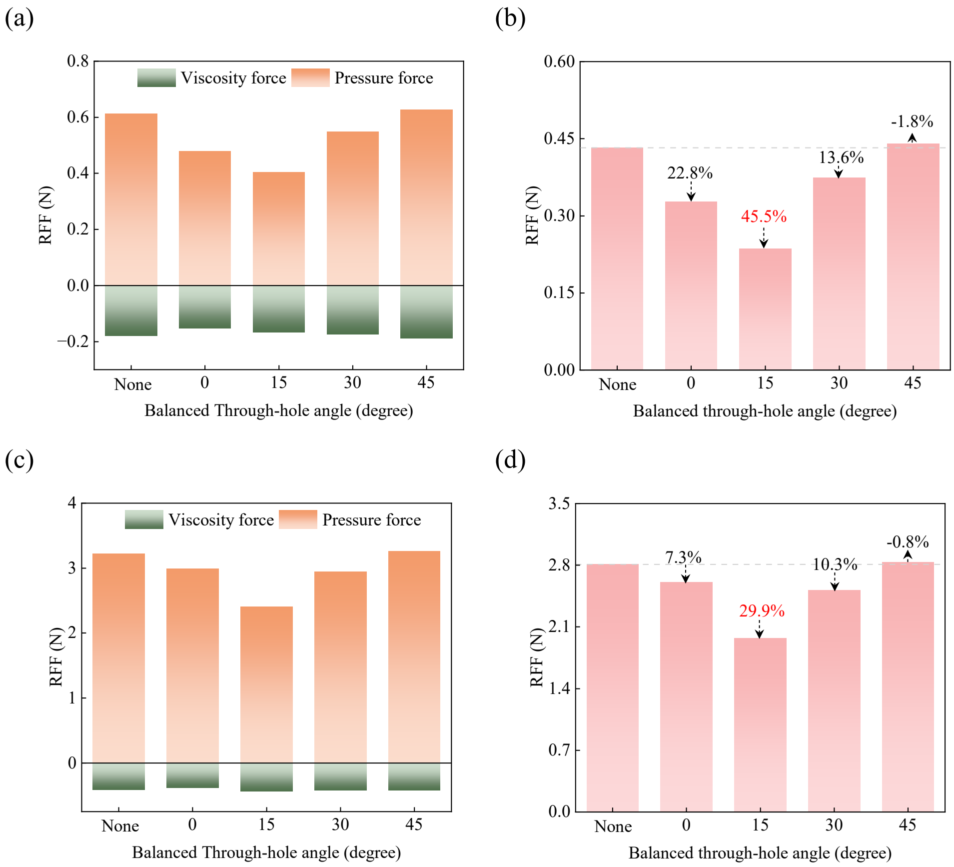

Figure 4.9. RFF (F_r) on the middle shoulder wall (W_1) and overall wall (W_{all}) of different balanced through-hole angle model: (a) Pressure and viscosity RFF components of W_1; (b) Overall RFF of W_1; (c) Pressure and viscosity RFF components of W_{all}; (d) Overall RFF of W_{all}.

The spool RFFs (comprising pressure force and viscous force) for different through-hole angles are demonstrated in Figure 4.9. As illustrated in Figure 4.9(a) and (c), the pressure force component remains predominant in the RFF, and the trend in the performance of the pressure component for each angle structure is consistent with the trend in the total RFF change. The viscous force component is less affected by the through-hole angle and remains stable, indicating that the viscous effect varies weakly within the range of structural parameters in this study. As the through-hole angle is adjusted, the total RFF undergoes a corresponding alteration from Figure 4.9(b) and (d), reaching its most significant decline (W_1 reduce by 45.5% and W_{all} reduce by 29.9%) of D_2. This observation signifies a substantial RFF balancing effect. Notably, For D_4, the RFF approaches the level observed in a structure devoid of holes.

5. CONCLUSION

This study presents a comprehensive investigation of the generation and mitigation for unbalanced RFFs in open-neutral HSVs. Through detailed CFD simulations, the research reveals that RFF is primarily caused by asymmetric pressure distribution across the spool shoulder surfaces, especially in regions with strong vortex formation and abrupt geometric transitions. The viscous component, while present, is comparatively minor. A novel structural strategy introducing through-holes in the mid-shoulder region was proposed to alleviate this imbalance. These through-holes create a preferential flow path that effectively redistributes pressure, promotes local flow symmetry, and reduces radial pressure differentials. Among the tested configurations, the 15° inclined through-hole model demonstrated the most effective performance, reducing local middle shoulder RFF by up to 45.5% and total spool RFF by 29.9%.

In contrast to traditional groove-type pressure balancing methods, the proposed design is more adaptable to compact valve architectures and complex multi-step throttling geometries. It also avoids secondary pressure peaks often introduced by overly steep hole angles, thus ensuring stable flow transition and minimal disturbance. Experimental validation of the proposed through-hole design will be conducted in a subsequent stage of this research to further assess its effectiveness under practical operating conditions.

6. ACKNOWLEDGMENTS

This work was supported by the National Natural Science Foundation of China (Grant No. 52275008); and the Southern Marine Science and Engineering Guangdong Laboratory (Zhuhai) (Grant No. SML 2024SP007).

7. REFERENCES

[1] T. Lin, Y. Lin, H. Ren, H. Chen, Q. Chen, and Z. Li, ‘Development and key technologies of pure electric construction machinery’, Renew. Sustain. Energy Rev., vol. 132, pp. 110080, Oct. 2020.

[2] G. Zhang, K. Zhang, W. Shen, G. Xu, and Y. J. Lin, ‘Intelligent fault diagnosis of multi-way directional valves in hydraulic systems using digital twin and deep learning approaches’, Mech. Syst. Signal Process., vol. 230, pp. 112579, May 2025.
[3] L. Romagnuolo, R. De Rosa, E. Frosina, and A. Senatore, ‘Study of a proportional spool valve noise by means of functional data analysis: cavitation and intensity detection’, Mech. Syst. Signal Process., vol. 209, pp. 111100, Mar. 2024.
[4] W. Li, H. Jiang, C. Feng, Z. Wang, S. Ma, and X. Xu, ‘A hybrid intelligent diagnostic approach for spool jamming faults of hydraulic directional valves’, Measurement, vol. 241, pp. 115706, Feb. 2025.
[5] D. Li et al., ‘A prediction model of fluid–solid erosion wear in hydraulic spool valve orifice’, Wear, vol. 540–541, pp. 205235, Mar. 2024.
[6] M. Simic and N. Herakovic, ‘Reduction of the flow forces in a small hydraulic seat valve as alternative approach to improve the valve characteristics,’ Energy Conversion and Management, vol. 89, pp. 708–718, Jan. 2015.
[7] R. Amirante, E. Distaso, and P. Tamburrano, ‘Sliding spool design for reducing the actuation forces in direct operated proportional directional valves: Experimental validation’, Energy Conversion and Management, vol. 119, pp. 399–410, Jul. 2016.
[8] M. Yang, Y. Zhang, C. Ai, G. Yan, and W. Jiang, ‘Multi-objective optimisation of K-shape notch multi-way spool valve using CFD analysis, discharge area parameter model, and NSGA-II algorithm’, Eng. Appl. Comput. Fluid Mech., vol. 17, no. 1, pp. 2242721, Aug. 2023.
[9] Y. Zhang, S. Wang, J. Shi, and X. Wang, ‘Evaluation of thermal effects on temperature-sensitive operating force of flow servo valve for fuel metering unit’, Chin. J. Aeronaut., vol. 33, no. 6, pp. 1812–1823, 2020.
[10] W. Yang et al., ‘CFD-based axial steady-state hydrodynamic study and structural optimization of miniature switching valve’, Flow Measurement and Instrumentation, vol. 100, pp. 102744, Dec. 2024.
[11] S. H. Hong and K. W. Kim, ‘A new type groove for hydraulic spool valve’, Tribology International, vol. 103, pp. 629–640, Nov. 2016.
[12] T. A. Zaki, ‘Turbulence from an Observer Perspective,’ Annu. Rev. Fluid Mech., vol. 57, no. 1, pp. 311–334, Jan. 2025.
[13] S. Zhang, Z. Lin, S. Chen, Z. Jin, and J. Qian, ‘Unbalanced force analysis on valve core clamping in hydraulic spool valves’, Annals of Nuclear Energy, vol. 203, pp. 110505, Aug. 2024.
[14] Y. Zhang, B. Ding, and G. Yan, ‘Reduced-order estimation and optimisation of claw-shaped throttling notch via CFD analysis, surrogate models, and CCMO algorithm’, Eng. Appl. Comput. Fluid Mech., vol. 19, no. 1, p. 2444418, Dec. 2025.
[15] K. Zhang, D. Wu, J. Wang, and Y. Song, ‘Numerical and experimental investigation of cavitation characteristics of the electronic expansion valves’, Phys. Fluids, vol. 36, no. 4, pp. 45144, Apr. 2024.

Biographies

Yuhang Zhang received the B.Eng degree from Nanjing Institute of Technology, Nanjing, China in 2021 and the M.Eng degree from Yanshan University, Qinhuangdao, China in 2024. He is currently working toward the Ph.D. degree with Sun Yat-sen University, Shenzhen, China. His research interests include cavitation erosion of high-pressure flows in confined spaces, and high-performance hydraulic components.

Shipei Zheng received the B.Eng. degree in mechanical engineering from Wuhan University of Technology, Wuhan, China in 2020 and the M.Eng. degree in robotics engineering from King's College London, U.K., in 2021. He is currently working toward the Ph.D. degree with Sun Yat-sen University, Shenzhen, China. His research interests include electrical machines and drive, motion control and robot control.

Jiaxi Zhang received the B.Eng. degree in mechanical engineering from Sun Yat-sen University, China, in 2021. He is currently working toward the M.Eng. degree with Sun Yat-sen University, Shenzhen, China. His research interests include cavitation erosion of high-pressure flows in confined spaces, and high-performance hydraulic components.

Jianshe Feng received the Ph.D. degree from University of Cincinnati, USA, in 2020. He is currently an Associate Professor with the School of Advanced Manufacturing, Sun Yat-sen University, Shenzhen, China. His research interests focus on industrial artificial intelligence, intelligent monitoring and optimization of manufacturing processes, predictive maintenance, and industrial big data analytics.

Miao Yang received the Ph.D. degree in mechatronic engineering from Harbin Institute of Technology, Harbin, China, in 2019. He is currently an Associate Professor with the School of Advanced Manufacturing, Sun Yat-sen University, Shenzhen, China. His research interests include compliant mechanisms, precision motion systems, parallel and robotic manipulators, robot force control, and mechatronic system integration.

Guangwei Zhang received the Ph.D. degree in mechanical engineering from the University of Tokyo, Tokyo, Japan, in 2019. He is currently an Associate Professor with the School of Advanced Manufacturing, Sun Yat-sen University, Shenzhen, China. His research interests include electrostatic film actuators and motors, precision motion control, artificial muscles, and soft robotic systems.

Beichen Ding received the Ph.D. degree in mechanical engineering from the University of Bath, Bath, U.K., in 2019. Currently, he is an Associate Professor with the School of Advanced Manufacturing, Sun Yat-sen University, Shenzhen, China. He is a member of the Intelligent Fluid Power Control of CSME. His research interests include actuation and motion control of smart machine systems and robot-assisted machining and dynamic modeling of electrical drives.